Korean J. Chem. Eng., 32(12), 2501-2506 (2015)
DOI: 10.1007/s11814-015-0088-9

pISSN: 0256-1115
eISSN: 1975-7220

Micro- and mesoporous CuBTCs for CO_2/CH_4 separation

Hyung Chul Yoon*,‡, Phani Brahma Somayajulu Rallapalli*,‡, Sang Sup Han*, Hee Tae Beum*, Tae Sung Jung*, Dong Woo Cho*, Minsu Ko, and Jong-Nam Kim*,†**

*Petroleum and Gas Laboratory, Korea Institute of Energy Research, Daejeon 305-343, Korea
**Oil & Gas Process R&D Part, Central Research Institute, Samsung Heavy Industries Co., LTD., Seongnami-si 463-400, Korea
(*Received 10 February 2015 • accepted 23 April 2015*)

Abstract−Micro- and mesoporous CuBTCs, referred to as *micro*- and *meso*-CuBTCs, were synthesized, and tested for their capacity to adsorptively remove CO_2 from a binary mixture of CO_2-CH_4. Physicochemical analyses of the thermally treated Cu-BTCs were performed. The CO_2 and CH_4 adsorption isotherms for the Cu-BTCs at 25 °C in the pressure range 0-3 MPa were experimentally measured and implemented for calculating the CO_2/CH_4 selectivity as a function of pressure and CO_2 concentration using the ideal adsorbed solution theory (IAST). The CH_4 adsorption capacity of *meso*-CuBTC at 3 MPa was reduced to 43% of that of *micro*-CuBTC, whereas the CO_2 adsorption capacity of *meso*-CuBTC at 3 MPa was reduced to 27% of that of micro-CuBTCs. Consequently, *meso*-CuBTC shows a higher CO_2/CH_4 selectivity compared to *micro*-CuBTC. It was also found that the selectivity of the CuBTCs could be enhanced by lowering the partial pressure of CO_2. This was ascribed to the larger abatement of the adsorption capacity for CH_4 than for CO_2, resulting from a reduction of the interaction of CH_4 with the surface of pores of *meso*-CuBTC of which the pore size had been augmented.

Keywords: Microporous CuBTC, Mesoporous CuBTC, CO_2, CH_4, Ideal Adsorption Solution Theory

INTRODUCTION

Raw natural gas contains methane as its major component, but also contains considerable amounts of light and heavier hydrocarbons along with other contaminants, including CO_2, N_2, Hg, He, and H_2S. Among them, acid gases, including CO_2 and H_2S, are problematic because they become acidic and corrosive in the presence of water, thereby causing corrosion of the pipeline and equipment during down/upstream processing. Therefore, it is necessary to reduce the amount of CO_2 in raw natural gas to 2% and 50 ppm for pipeline transportation and liquefaction, respectively. Absorption, adsorption, cryogenic methods, membrane processes, and micro algal bio-fixation have all been used as acid gas removal technologies. Of these technologies, those based on adsorption have received significant interest because of the simplicity of adsorbent regeneration by thermal or pressure variation [1]. The possibility of using the adsorption process for the removal of CO_2 from raw natural gas has been investigated and various adsorbents including activated alumina [2,3], activated carbons [4-6], ion-exchange resins [7], zeolites [8-10], porous silicates [11-13], metal oxides [14-16], and organic-inorganic hybrid sorbents [17-19] have been studied to this effect. Metal-organic frameworks (MOFs), formed by the combination of metallic clusters with organic ligands, have attracted particular attention as novel adsorbents due to their large surface areas and pore volume [20-25]. The disadvantage of most microporous MOFs is their high CH_4 adsorption capacity at high pressures when they are implemented as adsorbents for removing acid gas from natural gas. This results in a high methane loss and a low selectivity for CO_2/CH_4. The pore size of an adsorbent is a key parameter that plays a significant role in determining the interaction of CH_4 molecules with the pore wall [26]; therefore, tailoring the pore size and metrics of the adsorbent is an important factor for optimizing an MOF for achieving effective adsorptive acid gas removal.

Among the MOFs reported to date, CuBTC (HKUST-1), a highly porous open-framework material with the formula $[Cu_3(BTC)_2(H_2O)_3]_n$ (BTC is 1,3,5-benzenetricarboxylate), is one of the first materials of this family to be produced on an industrial scale by BASF SE under the commercial name of Basolite C300 [27]. Detailed information on CuBTC can be found in [28]. Experimental studies on single component adsorption of CO_2 and CH_4 for CuBTC were reported [29-38]. Molecular simulation studies of the adsorption of CO_2-CH_4 binary mixtures predicted a high CO_2/CH_4 selectivity for CuBTC [39-43]. Hamon et al. [44] reported experimental data for the co-adsorption of CO_2-CH_4 binary mixtures for CuBTC. The pore size plays an important role in determining the selectivity of MOFs; therefore, tailoring the pore size of CuBTC for acid gas removal from natural gas is considered necessary for lowering the CH_4 adsorption capacity (i.e., reducing CH_4 loss), and enhancing the CO_2/CH_4 selectivity, and this remains unstudied to date.

In this contribution, micro- and mesoporous CuBTC were synthesized and physicochemically characterized by powder x-ray diffraction (PXRD), thermogravimetric analysis (TGA), BET surface area analysis, and pore volume/diameter analysis. The CO_2 and CH_4

†To whom correspondence should be addressed.
E-mail: jnkim@kier.re.kr
‡This article is dedicated to Prof. Hwayong Kim on the occasion of his retirement from Seoul National University.
‡H.C.Y. and P.B.S.R. contributed equally to this work.

adsorption capacities were measured at 25 °C in the pressure range 0-3 MPa. Additionally, the CO_2/CH_4 selectivity was estimated by using ideal adsorbed solution theory (IAST) on the basis of the single component isotherms for CO_2 and CH_4.

EXPERIMENTAL

1. Materials

Copper (II) nitrate trihydrate [$Cu(NO_3)_2 \cdot 3H_2O$ (Junsei Chemical, 98%)], 1,3,5-benzenetricarboxylic acid (H_3BTC) (Sigma Aldrich, 95%), and Cetyltrimethylammonium bromide (CTAB) ($(C_{16}H_{33})N(CH_3)_3Br$, Sigma Aldrich, 99%), 1,3,5-trimethylbenzene (TMB) (TCI Chemicals, >97%) and ethanol (Samchun Pure Chemical, >99.8%) were purchased.

1-1. Synthesis of Microporous CuBTC

The synthetic procedure was adopted from Hamon et al. [44] with minor changes. A 100 mL Teflon-lined steel bomb was charged with 25 mL ethanol to which 1.79 g of H_3BTC was added under stirring. Then 3.05 g of copper (II) nitrate trihydrate, dissolved in 25 mL water, was added to the ethanol/H_3BTC suspension and the reaction mixture was stirred for 30 min at ambient temperature. The bomb was sealed, placed in an oven, and heated at 120 °C for 18 h. The resulting blue crystals of Cu-BTC were isolated by filtration and washed with ethanol. This product was designated as *micro*-CuBTC and was dried for overnight at 70 °C.

1-2. Synthesis of Mesoporous CuBTC

The procedure for the synthesis of mesoporous CuBTC was adopted from Qiu et al. [45] with minor changes. A 100 mL Teflon-lined steel bomb was charged with 25 mL ethanol and placed on a magnetic stirrer, after which 1.79 g of benzene-1,3,5-tricarboxylic acid (H_3BTC) was added to the ethanol under stirring. Then 2.5 g of copper nitrate trihydrate [$Cu(NO_3)_2 \cdot 3H_2O$], dissolved in 25 mL water, was added to the ethanol/H_3BTC suspension, to which 1.13 g CTAB and 0.37 g TMB were subsequently added while stirring. The reaction mixture was stirred for 30 min at ambient temperature, after which the bomb was sealed, placed in an oven, and heated at 180 °C for 12 h. CuBTC, which precipitated as a blue powder, was isolated by filtration and washed with ethanol. The templates CTAB and TMB were removed by Soxhlet extraction for 24 h using ethanol. This product, which was designated as *meso*-CuBTC, was dried for overnight at 70 °C.

2. Measurements

The PXRD patterns for both the *micro*- and *meso*-CuBTC samples were measured at ambient temperature using a PHILIPS X'pert MPD diffractometer in the 2θ range 2-60° at a scan speed of 0.1°/s using CuKα1 (λ=1.54056 Å) radiation. The thermal stability of the CuBTC compounds was investigated by using TGA (Q50 V20.2 Build 27) at a heating rate of 1 °C/ min under an argon atmosphere in the temperature range 25-400 °C.

The BET surface area, pore volume, and pore diameter of the Cu-BTCs were determined in a static volumetric gas adsorption system (Micromeritics Instrument Corporation, USA, model ASAP 2020) using the N_2 adsorption-desorption isotherm in the pressure range 0-1 atm at 77.4 K. The BET equation, Horváth-Kawazoe (HK) method (cylinder pore geometry Saito-Foley), Barrett-Joyner-Halenda (BJH) desorption, and the single point adsorption methods were adapted to calculate the surface area, pore diameter, and pore volume, respectively. Prior to the aforementioned measurements, the samples were dried at 180 °C under vacuum (6.7×10^{-2} Pa) for 18 h. The actual weight of the dried sample was determined by obtaining the weight difference before and after drying. High-pressure CO_2 and CH_4 adsorption measurements were performed at 25 °C in the pressure range 0-3 MPa in an automated high-pressure gas adsorption system (BELSORP-HP, BEL Japan).

RESULTS AND DISCUSSION

The PXRD patterns of *micro*- and *meso*-CuBTCs are plotted in Fig. 1. The PXRD pattern of *micro*-CuBTC is in good agreement with that in previous literature [44]. The PXRD pattern of *meso*-CuBTC resembles that of *micro*-CuBTC without any changes in the positions of the peaks, but the intensity of the peaks was reduced, which indicated a less crystalline material compared with *micro*-

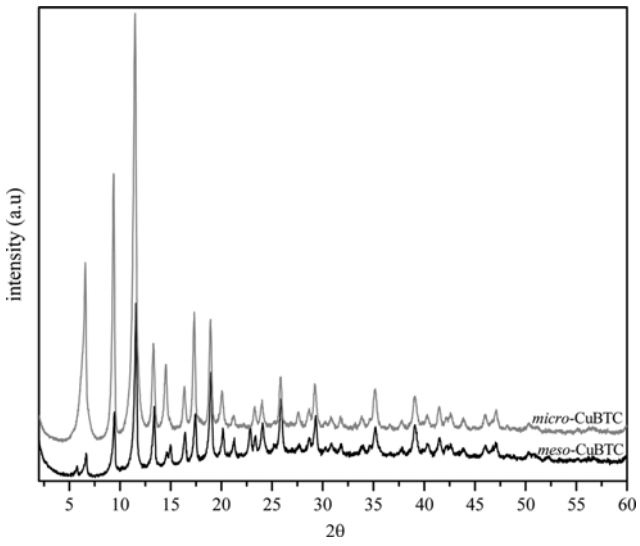

Fig. 1. Powder X-ray diffraction patterns of *micro*- and *meso*-CuBTC.

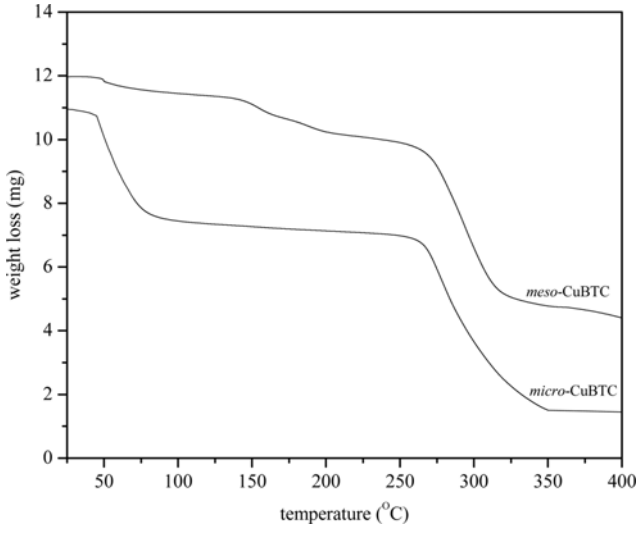

Fig. 2. TGA of *micro*- and *meso*-CuBTC.

CuBTC produces a disordered mesostructure [45].

The thermal stability of *micro*- and *meso*-CuBTC was analyzed by TGA and the result is shown in Fig. 2. Both CuBTCs display a weight loss in the temperature range 50-150 °C, which corresponds to a loss of surface-adsorbed ethanol and water molecules that were coordinated to Cu metal centers. A weight loss in the temperature range 150-230 °C indicates the loss of templates that were not removed by the Soxhlet extraction in the case of *meso*-CuBTC. From 300 °C onwards, the CuBTCs start to decompose. These results enabled us to conclude that the thermal stability of *meso*-CuBTC is not altered regardless of the introduction of mesoporosity.

Fig. 3 shows the N_2 adsorption-desorption isotherms of *micro*- and *meso*-CuBTC at 77.4 K and relative pressures (P/P_0) and the BET surface area, pore volume, and pore size values of the two compounds are given in Table 1. The isotherm of *micro*-Cu-BTC is of Type-I, which is indicative of its microporous nature. The isotherm of *meso*-CuBTC is of both Type-I and Type-IV, indicating that it has a combined mesoporous/microporous nature. *Meso*-CuBTC shows a steep uptake at very low P/P_0 (0.01), which is characteristic for microporous materials, and a hysteresis loop at P/P_0 0.5-0.9, which is characteristic for a mesoporous material [45]. The result also shows that the surface area of *meso*-CuBTC was reduced compared to that of *micro*-CuBTC. The total specific pore volume (V_t, determined by using the adsorption branch of the N_2 isotherm at $P/P^0=0.99$) of *micro* and *meso*-CuBTC was 0.58 and 0.54 cm^3/g, respectively. Although there is a difference between the nitrogen isotherms of *micro* and *meso*-CuBTC, as shown in Fig. 3, the total pore volume of these materials seems to be similar. To evaluate this, the specific mesopore and micropore volumes of *meso*-CuBTC were calculated. The specific mesopore volume (V_{meso}, determined from the BJH desorption cumulative volume of pores between 1.7 and 300.0 nm diameter) is 0.1 cm^3/g. The specific micropore volume (V_{micro}, calculated by subtracting V_{meso} from V_t) is 0.44 cm^3/g. The V_{meso}/V_{micro} ratio was found to be 0.23, which is similar to the value of 0.24 reported in [45]. Hence, the *meso*-CuBTC contains 81.48% micropore volume and 18.52% mesopore volume. Due to the high percentage of micropores, the total pore volume of *meso*-CuBTC appears to be similar to that of *micro*-CuBTC.

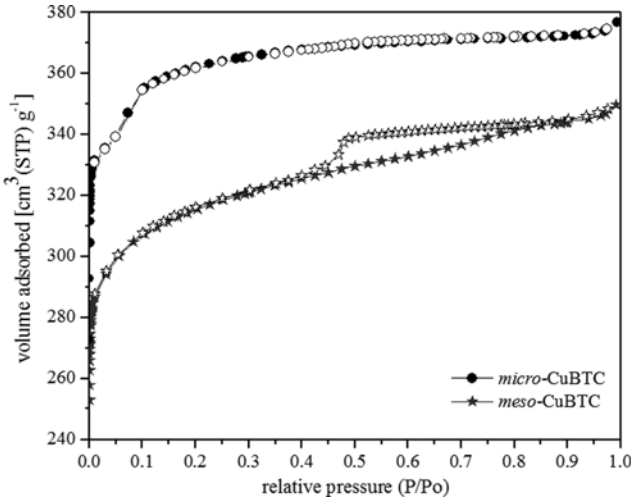

Fig. 3. N_2 adsorption-desorption isotherms of *micro*- and *meso*-CuBTC measured at 77 K in the relative pressure (P/P_0) range 0-1 (filled symbols for adsorption and empty symbols for desorption).

Table 1. Surface area, pore volume, and pore diameter of *micro*- and *meso*-Cu-BTC

Sample	S_{BET}[a] (m^2/g)	V_t[b] (cm^3/g)	Pore diameter (nm)
micro-CuBTC	1111.8	0.57	1.09[c]
meso-CuBTC	957.6	0.54	3.8[d]

[a]S_{BET} is the BET-specific surface area

[b]V_t is the total specific pore volume determined by using the adsorption branch of the N_2 isotherm at $P/P_0=0.99$

[c]Pore diameter calculated by HK method

[d]The mesopore diameter is determined from the local maximum of the BJH distribution of pore diameters obtained in the desorption branch of the N_2 isotherm

The pore size distribution (PSD) curves, which include the cumulative pore volume and its derivative with the pore diameter (dV/dD), were calculated by using the BJH method for *meso*- CuBTC and the curves are shown in Fig. 4. The *meso*-CuBTC shows a major peak at 3.8 nm. The PSD curves reveal the presence of mesopores in *meso*-CuBTC, for which the volume and diameter were calculated as 0.1 cm^3/g and 3.8 nm, respectively. The pore size of *micro*-CuBTC calculated by HK method is 1.09 nm, which is close to the value of 1.12 nm reported in [46].

The adsorption isotherms of CO_2 and CH_4 at 25 °C in the pressure range 0-3 MPa are shown in Fig. 5. The CO_2 adsorption capacity of *micro*-CuBTC and *meso*-CuBTC at 3 MPa was measured as 12.01 and 8.79 mmol/g, respectively. *Micro*-CuBTC displays a high CH_4 adsorption capacity of 7.9 mmol/g, which is in good agreement with the value found in a previous study [44]. The CO_2 and CH_4 adsorption capacity of *meso*- CuBTC at 3 MPa was 27 and

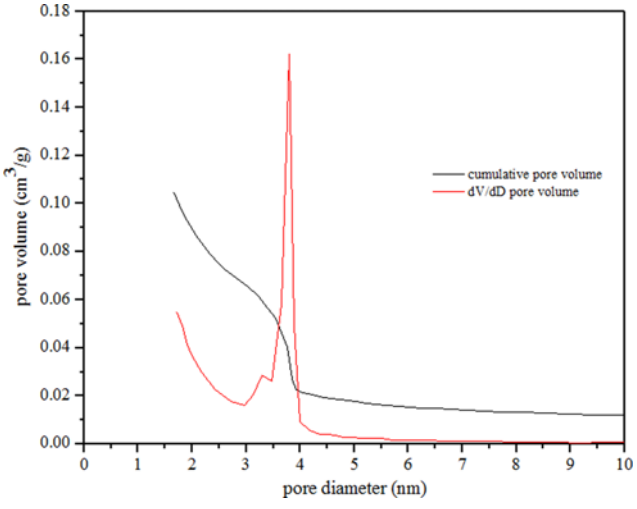

Fig. 4. Pore size distribution (PSD) curves including cumulative pore volume and its derivative with the pore diameter (dV/dD) calculated by the BJH method for *meso*-CuBTC.

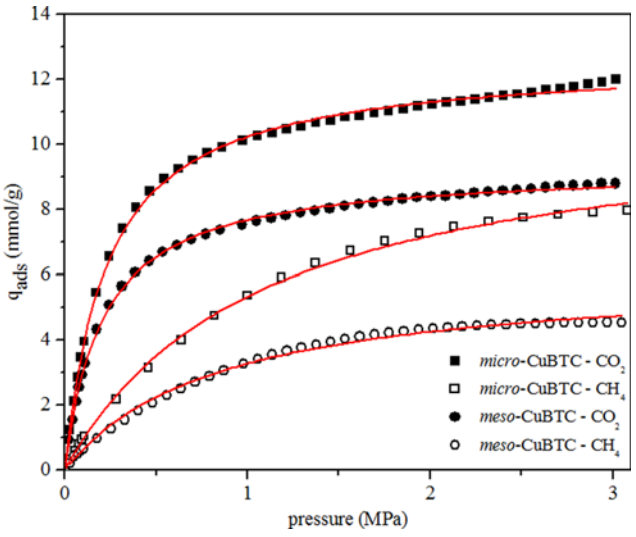

Fig. 5. CO_2 and CH_4 adsorption isotherms of *micro*- and *meso*-CuBTC measured at 25 °C in the pressure range 0-3 MPa (symbols for experimental data and solid red lines for SSLF fit).

43% less than those of *micro*-CuBTC, respectively. The pore size of an adsorbent is a key parameter that plays a significant role in determining the interaction of target molecules, in this case CH_4, with the pore wall. It was found that, in microporous adsorbents, at high pressure the overlapping force fields of the opposing micropore walls enhances the adsorption potential and facilitates the adsorption of supercritical CH_4 even at room temperature [26]. The CO_2/CH_4 selectivity for different compositions of CO_2-CH_4 binary gas mixtures was estimated from pure-component isotherms by using the ideal adsorbed solution theory (IAST), which was described by Myers and Prausnitz [46], and provides a convincing strategy by which to anticipate the adsorption selectivity and the adsorption equilibria of gas mixtures from the pure-component isotherm data. However, the use of this technique to estimate the selectivity requires good quality adsorption isotherm data of pure-component gases and a good curve-fitting model. The ease of this method, which requires no experimental data for the mixture, makes it particularly advantageous for engineering applications [47]. The ability of IAST to precisely predict gas mixture adsorption in various zeolites and MOF materials was reported previously [24,48-50].

Hamon et al. [44] utilized the dual-site Langmuir equation to fit the pure-component CO_2 and CH_4 isotherms. However, the fit results in identical values for the affinity coefficients of the two kinds of adsorption sites, which is comparable to using the single-site Langmuir equation. Obtaining a distinct segregation of the adsorption isotherms of the two adsorption sites is considered impractical [44].

Table 3. CO_2/CH_4 selectivity of the CuBTCs using IAST for 2-98% CO_2-CH_4 mixtures at 25 °C in the pressure range 0-3 MPa

Feed gas pressure (MPa)	CO_2/CH_4 IAST selectivity	
	micro-CuBTC	*meso*-CuBTC
0.1	197.16	230.65
0.5	119.84	142.67
1.0	93.89	114.64
1.5	82.93	103.02
2.0	76.89	96.67
2.5	73.06	92.66
3.0	70.42	89.90

In this work, he single-site Langmuir–Freundlich (SSLF) equation was capable of successfully fitting the single component isotherm data for CO_2 and CH_4.

The SSLF model can be expressed as follows:

$$q=q_m bp^{1/n}/(1+bp^{1/n}) \quad (1)$$

where p is the pressure of the bulk gas at equilibrium with the adsorbed phase (MPa), q is the adsorbed amount per mass of adsorbent (mmol/g), q_m is the saturation capacity (mmol/g), b is the affinity coefficient (MPa^{-1}), and n represents the deviations from an ideal homogeneous surface. Fig. 5 shows the experimental and calculated CO_2 and CH_4 adsorption isotherms of micro-CuBTC and *meso*-CuBTC, where the red solid line represents the SSLF model fit. The fitting parameters for the SSLF model, including the correlation coefficients (R^2), are tabulated in Table 2. The R^2 values obtained for all the fits are close to 0.99, which indicates that the SSLF model can be applied favorably for fitting the experimental CO_2 and CH_4 adsorption data.

The adsorption selectivity, S_{ads}, for CO_2-CH_4 binary mixture is defined as

$$S_{ads}=\frac{q1}{q2}\times\frac{p2}{p1} \quad (2)$$

where q1 and q2 represent the quantity of adsorbed CO_2 and CH_4, respectively, and p1 and p2 represent the partial pressures of CO_2 and CH_4, respectively.

The applicability of both *micro*- and *meso*-CuBTCs for polishing natural gas streams with a CO_2 content of 2% (i.e., pipeline (2% CO_2) to LNG quality (50 ppm CO_2)) was examined by using a binary mixture composition of 2-98% CO_2-CH_4. The CO_2/CH_4 selectivity of the CuBTCs as estimated by IAST for 2-98% CO_2-CH_4 mixtures at 25 °C in the pressure range 0-3 MPa is shown in Fig. 6 and tabulated in Table 3. The results show a reduction in the adsorption selectivity with an increase in the pressure. More importantly, the

Table 2. The SSLF fitting parameters for CO_2 and CH_4 adsorption on *micro*- and *meso*-CuBTCs

Sample	CO_2			CH_4		
	q (mmol/g)	b (MPa^{-1})	R^2	q (mmol/g)	b (MPa^{-1})	R^2
micro-CuBTC	12.60	4.34	0.9987	11.03	0.94	0.9983
meso-CuBTC	9.27	4.81	0.9991	6.06	1.18	0.9951

selectivity of *meso*-CuBTC was always determined to be higher than that of *micro*-CuBTC. The CO_2/CH_4 selectivity difference between the CuBTCs at 0.1 and 3 MPa is 33.49 and 19.48, respectively. The higher selectivity for CO_2 at 0.1 MPa might be a result of its high affinity for the CuBTCs owing to its quadrupole moment, whereas CH_4 does not have any quadrupole moment. The higher CO_2/CH_4 selectivity of *meso*-CuBTC compared to that of *micro*-CuBTC is presumably due to a decrease in the interaction between CH_4 and the pore walls as the pore size increases. On the other hand, an increase in the interaction between CH_4 and the pore walls as a result of increasing pressure could lead to an abatement of the CO_2/CH_4 selectivity, as shown in Fig. 6.

The CO_2/CH_4 selectivity for 1-5% CO_2 as estimated using IAST at 25 °C at 3 MPa is plotted in Fig. 7 and tabulated in Table 4. The selectivity of *meso*-CuBTC is higher than that of *micro*-CuBTC under the given conditions, reaching a selectivity of 142.27 and 181.63

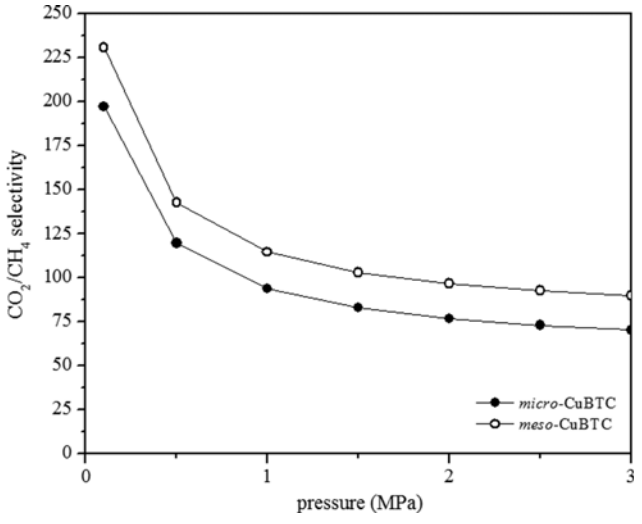

Fig. 6. CO_2/CH_4 selectivity for a 2-98% CO_2-CH_4 mixture estimated from IAST at 25 °C and in the pressure range 0-3 MPa.

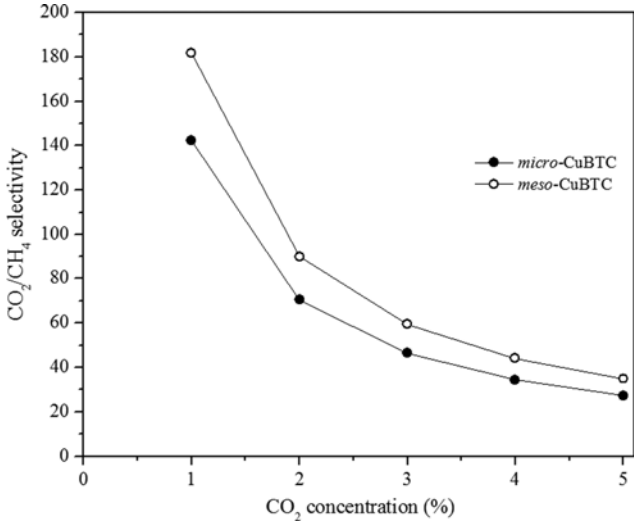

Fig. 7. CO_2/CH_4 selectivity for 1-5% CO_2 estimated using IAST at 25 °C and 3 MPa.

Table 4. CO_2/CH_4 selectivity for 1-5% CO_2 estimated using IAST at 25 °C and 3 MPa

Feed gas concentration (%)		CO_2/CH_4 IAST selectivity	
CO_2	CH_4	*micro*-CuBTC	*meso*-CuBTC
1.0	99.0	142.27	181.63
2.0	98.0	70.42	89.90
3.0	97.0	46.46	59.32
4.0	96.0	34.49	44.03
5.0	95.0	27.30	34.86

CO_2/CH_4 (1% CO_2) for *micro*- and *meso*-CuBTCs, respectively. The selectivity of the CuBTCs decreases with increasing CO_2 concentration, because of the saturation of the strongly adsorbing sites on the surface at the higher partial pressure of CO_2 in the feed gas mixture. However, lowering the CO_2 concentration further would substantially increase the CO_2/CH_4 selectivity, because of the comparatively higher adsorption capacity of CO_2 in the low-pressure region.

CONCLUSIONS

Two adsorbents, *micro- and meso*-CuBTC, were synthesized and tested for their ability to selectively remove CO_2 from a binary mixture of CO_2-CH_4. The PXRD, TGA, and BET measurements revealed that *meso*-CuBTC, of which the pore size had been tailored, was successfully synthesized with a slight reduction in its BET surface area, while maintaining its thermal stability. The isotherms of CO_2 and CH_4 were experimentally measured in the pressure range 0-3 MPa and implemented for calculating the CO_2/CH_4 selectivity using the IAST. Even though *meso*-CuBTC exhibited lower CO_2 and CH_4 adsorption capacities than *micro*-CuBTC, the CO_2/CH_4 selectivity of *meso*-CuBTC is higher than that of *micro*-CuBTC, owing to a larger abatement of the adsorption capacity for CH_4, resulting from a reduction in the extent to which CH_4 interacts with the walls of the pores of *meso*-CuBTC, which have an augmented size.

ACKNOWLEDGEMENT

This work was supported by the Global Leading Technology Program of the Office of Strategic R&D Planning (OSP) funded by the Ministry of Knowledge Economy, Republic of Korea (10042424).

REFERENCES

1. S. Choi, J. H. Drese and C. W. Jones, *ChemSusChem*, **2**, 796 (2009).
2. S. C. Lee, Y. M. Kwon, C. Y. Ryu, H. J. Chae, D. Ragupathy, S. Y. Jung, J. B. Lee, C. K. Ryu and J. C. Kim, *Fuel*, **90**, 1465 (2011).
3. J. V. Veselovskaya, V. S. Derevschikov, T. Y. Kardash, O. A. Stonkus, T. A. Trubitsina and A. G. Okunev, *Int. J. Greenh. Gas Control*, **17**, 332 (2013).
4. S. Sircar, T. C. Golden and M. B. Rao, *Carbon*, **34**, 1 (1996).
5. C. Pevida, M. G. Plaza, B. Arias, J. Fermoso, F. Rubiera and J. J. Pis, *Appl. Surf. Sci.*, **254**, 7165 (2008).

6. M. G. Plaza, C. Pevida, A. Arenillas, F. Rubiera and J. J. Pis, *Fuel*, **86**, 2204 (2007).
7. W. R. Alesi and J. R. Kitchin, *Ind. Eng. Chem. Res.*, **51**, 6907 (2012).
8. H. Maghsoudi, M. Soltanieh, H. Bozorgzadeh and A. Mohamadalizadeh, *Adsorption*, **19**, 1045 (2013).
9. J. Zhang, R. Singh and P. A. Webley, *Micropor. Mesopor. Mater.*, **111**, 478 (2008).
10. S. Cavenati, C. A. Grande and A. E. Rodrigues, *J. Chem. Eng. Data*, **49**, 1095 (2004).
11. Y. Belmabkhout, G. D. Weireld and A. Sayari, *Langmuir*, **25**, 13275 (2009).
12. R. S. Franchi, P. J. E. Harlick and A. Sayari, *Ind. Eng. Chem. Res.*, **44**, 8007 (2005).
13. X. Ma, X. Wang and C. Song, *J. Am. Chem. Soc.*, **131**, 5777 (2009).
14. Z. Yong, V. Mata and A. E. Rodrigues, *Sep. Purif. Technol.*, **26**, 195 (2002).
15. M. Kato, S. Yoshikawa and K. Nakagawa, *J. Mater. Sci. Lett.*, **21**, 485 (2002).
16. K. Nakagawa and T. Ohashi, *J. Electrochem. Soc.*, **145**, 1344 (1998).
17. R. Chatti, A. K. Bansiwal, J. A. Thote, V. Kumar, P. Jadhav, S. K. Lokhande, R. B. Biniwale, N. K. Labhsetwar and S. S. Rayalu, *Micropor. Mesopor. Mater.*, **121**, 84 (2009).
18. T. Tsuda and T. Fujiwara, *J. Chem. Soc., Chem. Commun.*, 1659 (1992).
19. O. Leal, C. Bolívar, C. Ovalles, J. J. García and Y. Espidel, *Inorg. Chim. Acta*, **240**, 183 (1995).
20. G. Ferey, *Chem. Soc. Rev.*, **37**, 191 (2008).
21. U. Mueller, M. Schubert, F. Teich, H. Puetter, K. Schierle-Arndt and J. Pastre, *J. Mater. Chem.*, **16**, 626 (2006).
22. J.-R. Li, R. J. Kuppler and H.-C. Zhou, *Chem. Soc. Rev.*, **38**, 1477 (2009).
23. R. J. Kuppler, D. J. Timmons, Q.-R. Fang, J.-R. Li, T. A. Makal, M. D. Young, D. Yuan, D. Zhao, W. Zhuang and H.-C. Zhou, *Coord. Chem. Rev.*, **253**, 3042 (2009).
24. Y.-S. Bae, O. K. Farha, A. M. Spokoyny, C. A. Mirkin, J. T. Hupp and R. Q. Snurr, *Chem. Commun.*, 4135 (2008).
25. Y.-S. Bae, K. L. Mulfort, H. Frost, P. Ryan, S. Punnathanam, L. J. Broadbelt, J. T. Hupp and R. Q. Snurr, *Langmuir*, **24**, 8592 (2008).
26. V. C. Menon and S. Komarneni, *J. Porous. Mater.*, **5**, 43 (1998).
27. A. U. Czaja, N. Trukhan and U. Muller, *Chem. Soc. Rev.*, **38**, 1284 (2009).
28. S. S.-Y. Chui, S. M.-F. Lo, J. P. H. Charmant, A. G. Orpen and I. D. Williams, *Science*, **283**, 1148 (1999).
29. Q. M. Wang, D. Shen, M. Bülow, M. L. Lau, S. Deng, F. R. Fitch, N. O. Lemcoff and J. Semanscin, *Micropor. Mesopor. Mater.*, **55**, 217 (2002).
30. Z. Liang, M. Marshall and A. L. Chaffee, *Energy Fuels*, **23**, 2785 (2009).
31. E. García-Pérez, J. Gascón, V. Morales-Flórez, J. M. Castillo, F. Kapteijn and S. Calero, *Langmuir*, **25**, 1725 (2009).
32. A. R. Millward and O. M. Yaghi, *J. Am. Chem. Soc.*, **127**, 17998 (2005).
33. D. Farrusseng, C. Daniel, C. Gaudillère, U. Ravon, Y. Schuurman, C. Mirodatos, D. Dubbeldam, H. Frost and R. Q. Snurr, *Langmuir*, **25**, 7383 (2009).
34. A. Ö. Yazaydın, A. I. Benin, S. A. Faheem, P. Jakubczak, J. J. Low, R. R. Willis and R. Q. Snurr, *Chem. Mater.*, **21**, 1425 (2009).
35. S. Cavenati, C. A. Grande, A. E. Rodrigues, C. Kiener and U. Müller, *Ind. Eng. Chem. Res.*, **47**, 6333 (2008).
36. I. Senkovska and S. Kaskel, *Micropor. Mesopor. Mater.*, **112**, 108 (2008).
37. P. Chowdhury, C. Bikkina, D. Meister, F. Dreisbach and S. Gumma, *Micropor. Mesopor. Mater.*, **117**, 406 (2009).
38. Y. Cheng, A. Kondo, H. Noguchi, H. Kajiro, K. Urita, T. Ohba, K. Kaneko and H. Kanoh, *Langmuir*, **25**, 4510 (2009).
39. R. Babarao, J. Jiang and S. I. Sandler, *Langmuir*, **25**, 5239 (2008).
40. Q. Yang and C. Zhong, *J. Phys. Chem. B*, **110**, 17776 (2006).
41. A. Martin-Calvo, E. Garcia-Perez, J. M. Castillo and S. Calero, *Phys. Chem. Chem. Phys.*, **10**, 7085 (2008).
42. R. Krishna, *J. Phys. Chem. C*, **113**, 19756 (2009).
43. S. Keskin, J. Liu, J. K. Johnson and D. S. Sholl, *Micropor. Mesopor. Mater.*, **125**, 101 (2009).
44. L. Hamon, E. Jolimaître and G. D. Pirngruber, *Ind. Eng. Chem. Res.*, **49**, 7497 (2010).
45. L.-G. Qiu, T. Xu, Z.-Q. Li, W. Wang, Y. Wu, X. Jiang, X.-Y. Tian and L.-D. Zhang, *Angew. Chem. Int. Ed.*, **47**, 9487 (2008).
46. K. W. Chapman, G. J. Halder and P. J. Chupas, *J. Am. Chem. Soc.*, **130**, 10524 (2008).
47. A. L. Myers and J. M. Prausnitz, *AIChE J.*, **11**, 121 (1965).
48. R. Krishna and J. R. Long, *J. Phys. Chem. C*, **115**, 12941 (2011).
49. P. Ryan, O. K. Farha, L. J. Broadbelt and R. Q. Snurr, *AIChE J.*, **57**, 1759 (2011).
50. Z. Zhang, J. Liu, Z. Li and J. Li, *Dalton Trans.*, **41**, 4232 (2012).